LAWRENCE
LIVERMORE
NATIONAL
LABORATORY

LLNL-TR-663490

Novel Multiple - Gigahertz Electron Beams for Advanced X--Ray and Gamma - Ray Light Sources

D. Gibson

October 29, 2014

Disclaimer

This work performed under the auspices of the U.S. Department of Energy by Lawrence Livermore National Laboratory under Contract DE-AC52-07NA27344.

12-ERD-040

Novel Multiple-Gigahertz Electron Beams for Advanced X-Ray and Gamma-Ray Light Sources

Final Report

October 29, 2014

Motivation

Current and future generations of advanced light sources largely depend on high brightness electron beams. LLNL has spent the past decade developing Mono-Energetic Gamma-ray (MEGa-ray) sources by scattering laser light off an electron beam [1,2] for nuclear physics applications. At the SLAC National Accelerator Laboratory, the Linac Coherent Light Source (LCLS) is generating extraordinarily high peak brightness x-ray beams useful for biological, chemical, and physics studies by passing a 13.6 GeV electron beam through a series of magnetic undulators to form a Free-Electron Laser (FEL) [3]. Los Alamos is in the process developing the "MaRIE" (Matter-Radiation Interactions in Extremes) concept, which will also rely on FELs [4].

All these light sources would benefit from improved average brightness by increasing the repetition rate of the electron beam source. Since the undulators are based on permanent magnets, they will generate x-rays from as many electron bunches as can be delivered. Similarly, for MEGa-ray sources very little laser light is scattered from each individual electron bunch. If there are additional electron bunches to see the laser, they will also scatter photons, generating more gamma-rays. Modeling has shown that using trains of hundreds of electron bunches allows high gamma-ray fluxes to be generated using ns-long scattering laser pulses. This means that chirped pulse amplification would not be needed for the interaction laser, considerably simplifying the architecture. This would also allow for lower laser bandwidth at the interaction point, along with a larger focal spot size, eliminating the laser contribution to the scattered gamma-ray bandwidth. Additionally, lower charge per bunch allows more flexibility in the transport, simplifying efforts to mitigate noise-inducing dark current.

The overarching goal of the proposed research is to develop and demonstrate the required technology to generate multi-GHz rep-rate electron beams at pC-scale bunch charges to allow 100x increases in the average beam current. To achieve this, the project consisted of two major efforts:

1. Demonstration of a photocathode drive laser capable of generating the electron beam.
2. Commissioning of an x-band accelerator to enable studies of inter-bunch electromagnetic field interactions.

Excellent results were achieved in both areas.

Photoinjection Drive Laser

The goal of the Photoinjection Drive Laser portion of the research was a reduction to practice of a patent that the laboratory has filed (Application 20110168888) by

demonstrating the generation of an sub-ps laser pulse train of several hundred pulses with 11 GHz spacing. This beam was generated from a CW source laser modulated by an RF signal that would also drive the accelerator to guarantee synchronization, and the bandwidth to generate the short pulse would be generated via self-phase modulation in a few hundred meters of optical fiber. The system would be all fiber based except for the final small bulk-optic grating compressor. The scientific details are presented in the attached article published in *Optics Letters* in 2013, "Widely tunable 11 GHz femtosecond fiber laser based on a nonmode-locked source."

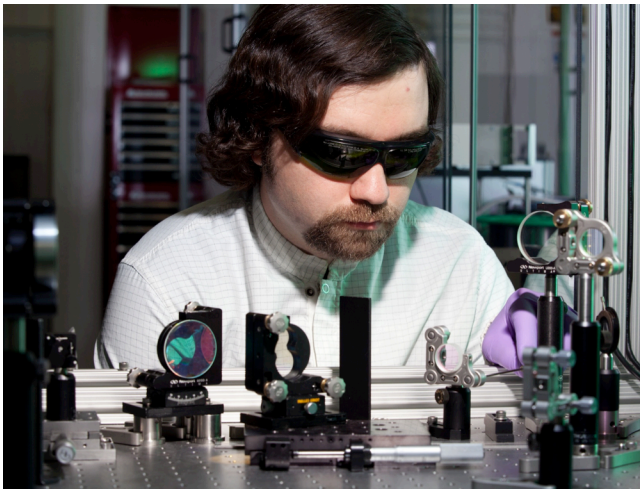

Lab physicist Matt Prantil aligns the GHz Photoinjection Drive Laser compressor. Because the chirp generated by self-phase modulation in the fiber system is small, only a small compressor is required.

Subsequent to the publication of the results in the paper, we further demonstrated micropulse energies of up to 5 μJ, corresponding to a macropulse energy of 2.5 mJ. This energy is sufficient to allow generation of 25 pC electron bunches on a Mg photocathode with a quantum efficiency of 10^{-4}, and therefore meets the design requirements of the laser.

X-Band Accelerator

The largest portion of the effort of this ER went into standing up the x-band accelerator system in the south cave of the B194 accelerator complex. This has resulted in a world-class system with a unique pairing of high-stabilty RF power with a state of the art X-band photoinjector and acceleration section, coupled with a comprehensive control system and drive and scattering laser systems to generate electrons and x-rays, respectively. At least three peer-reviewed publications are envisioned to result from this work: a NIMA paper detailing the RF source and modulator, a NIMA detailing commissioning of the linac, and a PRSTAB or NIMA on first X-band photoinjector results. Preliminary results that will be finalized as part of paper preparation and peer-review commentary are discussed here. This work included the commissioning of the high-power RF system to drive the accelerator, installation and commissioning of the accelerator structures, electron generation and scattering laser system delivery, and electron beam generation and characterization.

Klystron Commissioning

The power for the electron beam comes from a SLAC National Accelerator Laboratory XL-4 klystron. Developed as part of the Next Linear Collider program at SLAC in the 1990s, the XL-4 amplifier is capable of producing 50 MW RF power for 1.6 microseconds at 11.424 GHz. The installation at LLNL takes this limited production tube (~30 completed) a step further with the use of a state-of-the-art solid-state modulator to produce incredibly reliable high voltage pulses, which because of the dependence of klystron gun beam current on voltage produces very reliable RF power. This is the second installation of this kind in the world, and the only accelerator using this combination to produce high quality electron beams.

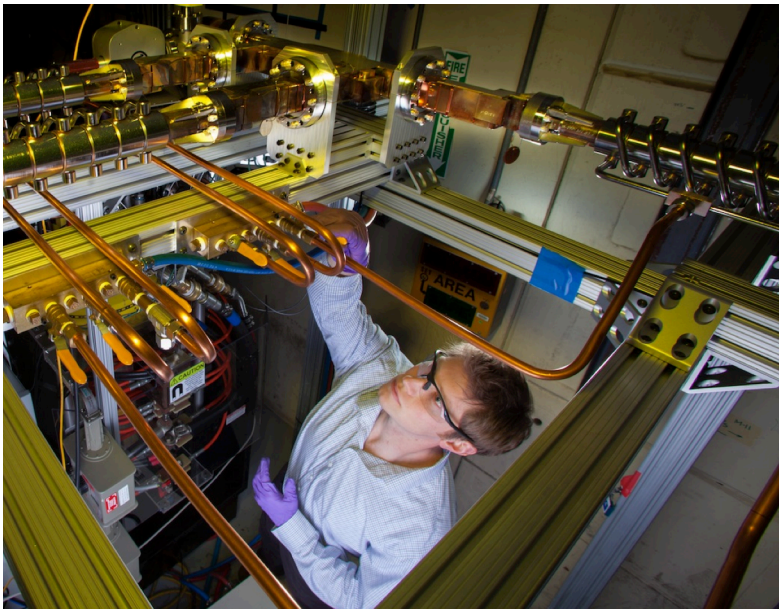

Lab physicist Roark Marsh assembles the RF testing structure used to commission the modulator and 50 MW klystron.

The XL-4 klystron was full high voltage and high power RF conditioned as part of its production at SLAC. In order to power the tube at LLNL we completed a number of preliminary upgrades and measurements on the high voltage modulator: redundant interlocks were put in place to prevent unwanted power supply behavior; low inductance cables replaced the sixty 1 kV cables running from the modulator IGBTs to the pulse transformer tank; tuners were installed on each of the cable inputs based on measurements at CERN to provide a flatter high voltage pulse; several pumps were replaced with more robust models; a high voltage divider was designed, built and used to calibrate the capacitive voltage dividers used to measure the high voltage pulse during normal operation; all interlocks were double checked for functionality; and several software upgrades were completed.

The Scandinova provided control software was used throughout operation, and was found adequate to providing all necessary information and interface. One important feature that was implemented procedurally was ramping the gun heater filament current. An operating set point of 22A was determined at SLAC to be optimal for reliable thermionic emission from the klystron gun. Voltage versus current curves were measured for slow warm up times to allow for full heating of the gun structure. These curves determined that 15-16A was sufficient for warm up of the gun, without heating the cathode enough for depletion of the dispenser material. “Warm standby” of the machine has used this 16A breakpoint in order to prolong the lifetime of the tube by avoiding the thermal stress of a full cool down and warm up cycle, without cathode depletion.

The tube was installed without incident thanks in large part to engineering efforts in designing a shock reducing platform for transport and final installation of the klystron. The tube was dressed with lead shielding in a high bay with sufficient overhead access and then loaded onto the cart for final transport. Installation of the tube left a small rotational misalignment, which was corrected for in the final RF distribution with a custom bent waveguide piece, and in initial testing by rotating the entire load tree assembly.

Initial testing of the klystron was into a load tree made up of two medium high power water-cooled stainless loads. The power was split into the two loads using an overheight -3dB coupler capable of handling several hundred MW. Diagnostics were calibrated for RF and HV measurements during processing, and after vacuum baking the entire system 10^{-8} Torr vacuum levels were achieved. Processing of the klystron at LLNL proceeded at 10 Hz, due to ES&H safety concerns over personnel fire protection in B194, to an ultimate pulse length of 400 ns at the full 50 MW power level. Extremely good stability and flatness were measured, meeting all requirements for ideal linac integration and operation. The high voltage pulse flatness was measured to be 0.05%, which resulted in a measured RF flatness of 0.1%. Shots were extremely stable with 0.01% shot-to-shot jitter, with a phase stability of <0.5° which was limited by the systematic error of the measurement method.

The RF pulse shape included rising and falling edge features that were not a direct result of the HV and RF systems, but were a product of the load tree components or their assembly. In situ cold test measurements were completed after testing to confirm reflections were present from the load tree that caused transient reflections from the frequency content of the sharp edge pulse. The loads are reasonably broad band around 11.424 GHz, and the WR-90 and overmoded round waveguide are both used well inside their frequency bands, so very little response was expected. The entire assembly does represent a larger resonant structure, which could have natural modes excited by the high power RF; or a single flange could be poorly assembled resulting in a localized mismatch. In either case the pulse shape is not a limitation of the RF system, merely a feature of the specific testing method.

RF phase control was accomplished using an I/Q mixer in reverse, modifying an input RF signal by providing voltage on what are normally the output in-phase and quadrature-phase output arms of the hybrid splitter. This doubled as a pin switch providing <-30dB attenuation on the low level RF (LLRF) drive. An arbitrary function generator (AFG) was selected to drive the two arms based on bandwidth limited measurements attempting to produce as sharp a rise and fall on the modulated pulse as possible. It was determined that the I/Q mixers had an inherent bandwidth limitation of about 100 MHz, so a 100 MHz giga-sample (ns resolution) AFG was used. This identical setup can be modified for pulse flatness compensation by modifying the square pulses sent to the two I and Q arms. For multi-bunch operation this pulse flattening compensates for the beam loading inherent in accelerating multiple bunches, and allows the bunches to be maintained at exactly the same energy. Pulse shaping is also both necessary and ideal for RF compression schemes, in which phase flipping is required to operate the compression mechanism, but phase and amplitude shaping also serves to flatten the compressed

pulse shape. Long pulses in the full accelerator distribution exhibited a less than ideal return reflection, from either the tube itself, or more likely the RF distribution and mode converters near the klystron. This "nose" feature had small impact on the phase flatness of the RF pulse and was tolerated, and also avoided by using pulses of 120 ns or less for beam operation. In theory this pulse can be exactly compensated for in the LLRF using the AFG and hardware in place.

Accelerator Assembly and Conditioning

The test station was initially planned to be located in the North save of B194, but this was changed to the South cave to accommodate other experiments planned for the North cave. The change in location instigated a reevaluation of RF distribution plans and meant a shorter and less lossy transport could be built. A hole was bored in the wall between the magnet and south caves and overmoded 4.62" circular waveguide was used except for a mode converter pair used as 90° bend and to allow a bent WR90 piece to adjust for the misalignment of the klystron in its socket.

A full accelerator readiness review was required for the DOE approved commissioning of a new accelerator to begin. Approval was received and allowed RF conditioning to begin, because >10 MeV electrons would be created by accelerating dark current. Regular radiation surveys wee required and completed as the RF power and pulse length delivered to the T53 accelerating section and RF gun were increased to their nominal operating points. TLDs were distributed through the operating area to provide long terms maps of radiation levels. Completion of the DOE approved commissioning plan, along with all required surveys and results were consolidated in a report to DOE that the system is ready to begin "normal operations".

The photoinjector and T53 accelerator section were both designed to achieve accelerating gradients near 100 MV/m, which corresponds to 200 MV/m on the gun cathode surface. In order to reach these high surface field levels, a lengthy period of RF conditioning is required, processing through many breakdown events to reach

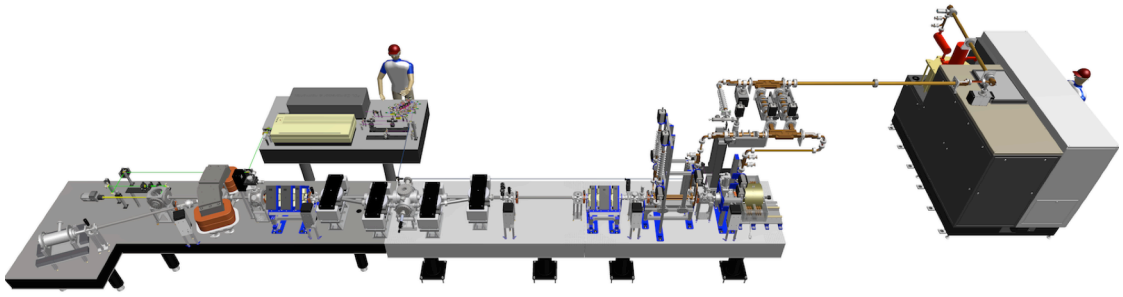

A CAD model of the x-band accelerator showing (right to left) the modulator and klystron, waveguide power distribution, photoinjector and T-53 accelerator section, noise mitigation chicane, focusing quadrupole magnets, interaction point, spectrometer/dump magnet, and beam dump. The back table holds the Nd:YAG interaction laser, as well as the compressor, frequency conversion, and pulse stacking hardware for the photoinjection drive laser.

higher and higher electric field levels with less chance of further breakdown and less emitted dark current. In order to avoid surface damage due to excessive breakdown, arc detection was performed using realtime LabView software. The arc detection program ran on a dedicated NI chassis that digitized the RF traces of interest and inhibited the system triggers in the case of a breakdown detection. Recovery varied from immediate turn on, or slow ramp back to full power, to prolonged shutdown for vacuum recovery.

The arc detection criteria was initially a channel by channel threshold detection that could be used to trigger on excessive dark current or large reflected power. A more subtle approach that was used for a long time was windowed threshold detection, so that noise on the trace outside the window of interest could be excluded, or so that the threshold could be set very low on the reflection by windowing in on the small region of highest breakdown activity. The most advanced criteria, which is currently the most reliable, combines threshold detection on traces such as the dark current and accelerating section reverse (which is typically quite small), with an absolute threshold on the integrated difference between one trace and the one immediately before it. This method is extremely sensitive to changes in reflected power so that small amounts of missing reflected power that feed a small breakdown event are detected and the system can avoid repeated high power arcing.

Conditioning of the photoinjector and accelerating structure took place in stages, so that the system could be broken in, radiation surveys could be performed, and the distribution waveguide components and vacuum system could be processed simultaneously. The section was processed to 25 MW at 250 ns, the highest power level it was likely to see in normal operation; this corresponds to an accelerating gradient of 50 MV/m, significantly de-rated from the high gradient testing this design has seen at 100+ MV/m, but with the benefit of very low breakdown rates and low dark current emission. The gun was processed up to 200 MV/m with and without the emittance compensation solenoid on, which was found to have a significant effect on breakdown physics.

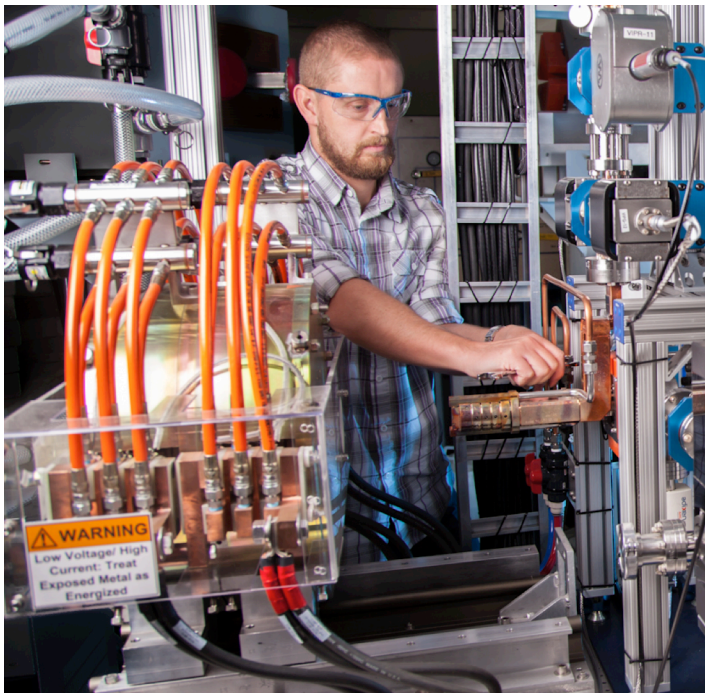

Mechanical engineer Scott Fisher makes the final cooling-water connections on the new x-Band photoinjection gun.

Three different varieties of breakdown were

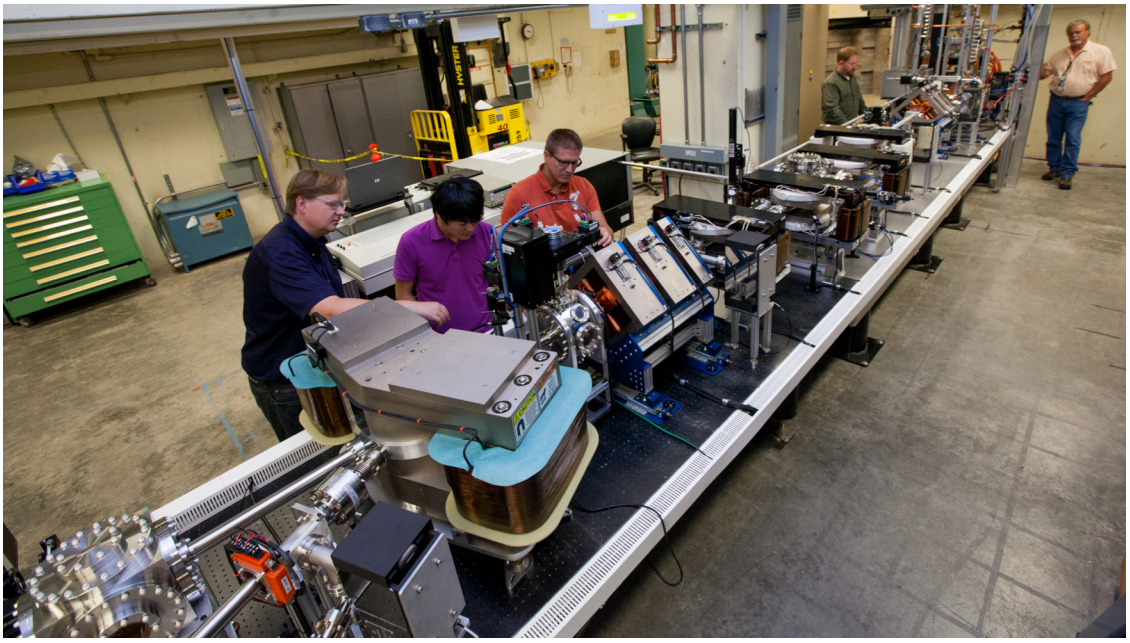

(L-R) Lab physicist Scott Anderson, summer student Yoonwoo Hwang (University of California, Irvine), laser technician Shawn Betts, project PI David Gibson, and linac operations manager Gerry Anderson finalize the installation of the new x-band accelerator in Building 194.

qualitatively observed during the gun processing, with quantitative analysis pending. Arcing on what was believed to be the medium power vacuum window on the gun input waveguide occurred reliably at peak input powers exceeding 20 MW. These were characterized by high frequency noise on the reflected diode, large power reflections to the T53 power arm of the divider, and no dark current. Breakdown on the cathode surface could be somewhat differentiated from arcing on the dual feed input coupler of the gun, but all high field breakdown events in the gun were similar. Breakdown occurring in the gun was also extremely sensitive to the presence of the emittance compensation solenoid. Ramping the field quickly is capable of causing arcs, and the breakdown events that occur with the solenoid on appear to cause more significant surface damage, requiring longer from which to recover. Once a gradient level was reached without the solenoid on, reprocessing was accomplished relatively quickly. The most expedient method for recovering from breakdown events was to recover from all arcs without the solenoid on. The system was then re-ramped with the solenoid on, once a comparable or slightly higher gradient was achieved with the solenoid off.

This is an important result for high gradient testing and breakdown physics that has been hinted at in low frequency testing 800 MHz gas filled structures, but not reproduced. In addition, this X-band RF photoinjector is a unique high gradient structure, and the breakdown statistics that have been accumulated support the international field in establishing metrics for design, performance, and physics models.

Laser systems

To generate the required electron beam, a UV laser required to liberate electrons from the copper photocathode in the photoinjector. Demonstrating the ideal, Multi-GHz, all-fiber drive laser was one of the goals of this ER, discussed above, and integrating that laser with this accelerator system is one of the next steps for future work. For purposes of commissioning and initial electron beam results, however, a commercial Ti:Sapphire laser system, which was part of a previous project to demonstrate inverse free electron laser activity, was used. That laser currently drives the S-Band photoinjector in B194. A pickoff mirror and a transport system to allow the beam to be redirected to the X-band accelerator area were installed, allowing the laser to be switched between accelerators with only a few minutes of effort. Near the X-band accelerator a dedicated pulse compressor and frequency tripler was installed to generate the beam required for electron generation. This provides up to 200 μJ of 261 nm light in a ~150-fs pulse. This pulse passes through a Michelson interferometer to allow us to generate two beams with adjustable timing, then is apertured to produce a sharp edge. The final beam is then relay-imaged onto the photocathode. Timing of the laser relative to the RF is controlled in the low-level RF system by adjusting the RF phase.

Additionally,an interaction laser was installed to allow for x-ray generation, which can be a valuable electron beam diagnostic. Ideally, this laser would be a Joule-level, few-ps long pulse. Work on previous LDRD and with external funding has demonstrated the feasibility of using diode-pumped Nd:YAG to meet these requirements, but integrating such a system was outside the budgetary scope of this project. Instead a spare commercial Nd:YAG laser, producing 800 mJ at 532 nm in a ~5 ns pulse was used. The beam energy is remotely controlled through a waveplate and polarizer pair along with ND filters. The beam is focused by a 1.5 m lens, then injected to the interaction region though the spectrometer dipole magnet. The spot size at the interaction is 100 μm, which modeling showed to be the optimal size for a long-pulse laser interacting with an electron beam. After the interaction, the light is collected by a mirror in the beam of the noise-mitigation chicane, discussed below, and extracted from the beamline.

Electron Beam results

First beam was immediately observed with the first RF to laser phase scan attempted; a testament to the precision alignment efforts that were made. Initial beam production informed the conditioning process and early attempts were made to measure and confirm the laser quality and electron beam energy. Initial measurements of quantum efficiency were extremely promising, revealing nearly five times the amount of charge expected for the given laser energy, and consistent with the best results achieved world-wide. First beam accelerated through the T53 section was as easily achieved on the first attempt, and allowed the gun to section phase to be calibrated. A rough energy measurement was used to estimate that an additional 45° of phase adjustment was necessary. Physical adjustments were made to the waveguide distribution to accomplish this, which was confirmed only once the entire system was complete and energy measurements were made with the

dump dipole magnet which functions once calibrated as an energy spectrometer.

Propagation through the entire system was attempted and achieved once the beam vacuum transport and laser interaction chambers were delivered and installed. The beam energy was measured at 28-30 MeV as expected, with the section phase adjustment for smallest energy spread occurring nicely in the middle of the phase shifter operating range. A minimal energy spread of 0.1% was measured with a jitter of 0.3%, most likely a combination of pointing jitter through the magnet and actual energy jitter.

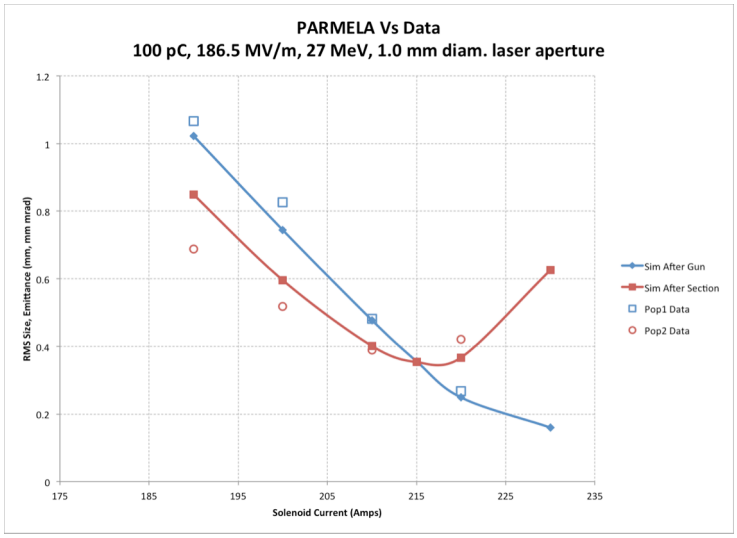

Electron spot size as a function of gun solenoid strength depends strongly on the gun gradient, and provides an additional verification of the field in the photoinjector.

Emittance measurements were one of the key confirmations of the photoinjector design, and an important metric for the quality of electron beam tune achieved. A quadrupole scanning technique was utilized in which the electron beam is measured on a phosphorescent screen while a quadrupole magnet is ramped. The resulting beam size versus field intensity data can be fit to electron beam propagation envelope equations, with the resulting fit parameters expressible as the electron beam alpha, beta, and normalized emittance (requiring the beam energy and current as additional input). Normalized RMS emittances of 0.8 mm mrad at 100pC and 0.4 mm mrad for 50 pC were ultimately measured once the system was tuned.

Electron beam tuning has focused on establishing the most central beam path through the photoinjector and accelerating section, and then the quadrupole triplets and chicane beamline onto the spectrometer screen. This path shows the least beam shape effect from RF phase change in the gun, solenoid field strength changes, gun to accelerator section phase change, and quadrupole field settings. The electron bunch normalized RMS emittance is the next most sensitive figure of merit for beam quality. Emittance measurement currently requires image saving for each magnet setting, image processing, and data fitting to beam envelope equations, in three distinct steps. This has made real-time emittance-based tuning difficult, but has been done to fine tune the two most critical emitance growth parameters: the laser spot position on the cathode, and the solenoid field strength.

The experimentally determined optimal solenoid field strength was found to be quite different from what was predicted by beam modeling simulations using PARMELA. In order to fit the data (shown in the figure), a higher peak electric surface field was required, and on reexamination, it was found that the RF gun

power measurement calibration was indeed underestimating the gradient by almost exactly what was predicted: the 165 MV/m point was in fact 190 MV/m.

During previous Compton scattering tests, we found that one of the largest noise sources was near-axis bremsstrahlung radiation from dark current in the gun and accelerator. To mitigate this problem, we installed a beam chicane after the acceleration section to divert the beam from, then return it to, the main line of propagation. This allows us to insert tungsten shielding material into the beamline to block this radiation. The chicane, assembled from parts reused from a previous LDRD project, was carefully designed to avoid any dispersion in the electron beam and to minimize any emittance growth as the beam passes through it.

The final electron beam requirement for Compton-scattering interaction is a tight spot on the interaction alignment cube, so that the electron bunch and laser beam can be collocated in space and time. A tight focus was established using the final focus quadrupole magnet triplet incrementally while maintaining a beam spot after the spectrometer magnet, in order to reduce any background x-ray flux from the spent beam. Optimal setting produced a small, bright spot of optical transition radiation (OTR) from the electron beam which could be viewed on the cube edge and aligned with the laser. The final achieved focus was on the order of 50 microns based on a preliminary calibration of the camera resolution.

Two-bunch demo

Once a single electron bunch tune had been established, two photocathode drive laser pulses were separated using a beam splitter and delay stage placed roughly one RF period away. RF phase was set using the fixed laser pulse, and the same phase was tuned using the translation of the stage for the same RF settings as the first pulse by blocking them one at a time. Acceleration was observed with both bunches, with all electron beam diagnostics registering twice the charge of each single bunch mode of operation. The beam image on the spectrometer was comparable to the single bunch case, with the stage mistuned in order to separate

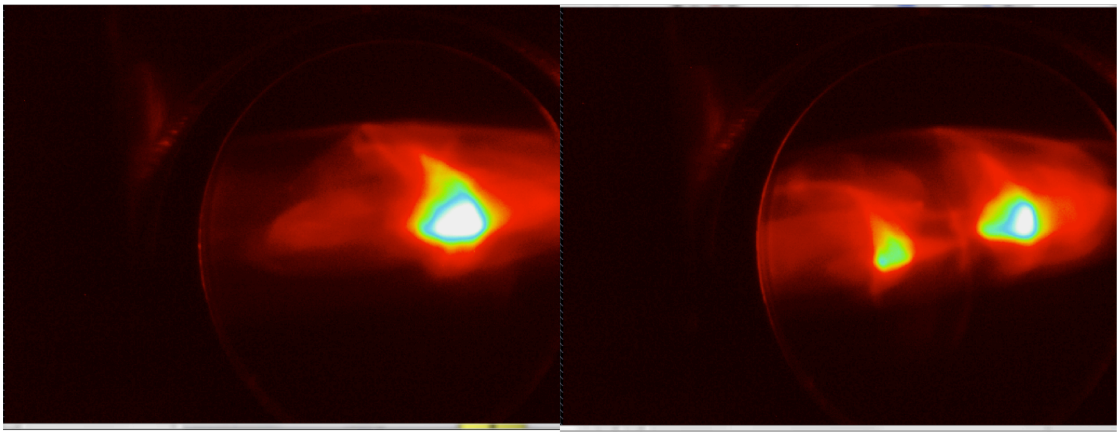

Two electron bunches, measured at 80 pC each, after a spectrometer magnet. (Left) the beams are overlapped in energy and (right) with one intentionally mistimed relative to the accelerating RF to show distinctly lower energy.

the two distinct beams in energy. Emittance data for the two simultaneous bunches was inconclusive as to emittance growth from the acceleration, but the data was promising and will be pursued further in the future.

Conclusions and Future Path

[Summary Paragraph]
[FROM WHITE PAPER] Following this demonstration, the next steps would be to secure support from a sponsor to implement the desired upgrade to the system end-point energy, brightness, and flux. To do so would include adding RF pulse compression to the RF distribution and extending the RF lines to reach an already-existing second section, enabling 100 keV x-ray production. Flux would be increased by replacing the current single-pulse, 10 Hz Ti:Sapphire system with the 120 Hz, multi-GHz pulse train drive laser currently sitting in B391, as well as moving the 120 Hz, 1-J interaction laser hardware, also demonstrated in B391, to B194.

Attachments

M. A. Prantil, E. Cormier, J. W. Dawson, D. J. Gibson, M. J. Messerly, and C. P. J. Barty, "Widely tunable 11 GHz femtosecond fiber laser based on a nonmode-locked source." *Optics Letters*, v. **38**, no. 17, p. 3216 (2013).

References

[1] D. J. Gibson et al., "Design and operation of a tunable MeV-level Compton-scattering-based gamma-ray source," *Phys Rev Spec. Top., Accel. and Beams*, vol. 13, p. 070703, 2010.

[2] F. Albert et al., "Design of narrow-band Compton scattering sources for nuclear resonance fluorescence," *Phys. Rev. ST Accel. Beams*, vol. 14, p. 050703, 2011.

[3] P. Emma et al., "First lasing and operation of an ångstrom-wavelength free-electron laser," *Nature Photonics*, vol. 4, pp. 641-647, 2010.

[4] B. E. Carlsten et al., "MaRIE X-Ray Free Electron Laser Pre-Conceptual Design," in *Proceedings of the 2011 Particle Accelerator Conference*, New York, 2011, p. TUODS1.